

1 **Does increasing horizontal resolution improve the**  
2 **simulation of intense tropical rainfall?**

3 **Akshaya C. Nikumbh<sup>1,2</sup>, Pu Lin<sup>1,2</sup>, David Paynter<sup>2</sup>, Yi Ming<sup>3</sup>**

4 <sup>1</sup> Atmospheric and Oceanic Sciences, Princeton University, Princeton, New Jersey

5 <sup>2</sup>Geophysical Fluid Dynamics Laboratory (NOAA), Princeton, New Jersey

6 <sup>3</sup>Schiller Institute for Integrated Science and Society, Boston College, Massachusetts

7 **Key Points:**

- 8 • Increasing horizontal resolution yields more intense tropical rainfall but not the  
9 accurate frequency distribution.
- 10 • Theoretical precipitation scaling accurately captures the frequency distribution  
11 of the simulated precipitation at moderate-to-high intensity
- 12 • Simulated precipitation extremes are more sensitive to the grid-scale updrafts than  
13 observed precipitation extremes

## Abstract

We examine tropical rainfall from Geophysical Fluid Dynamics Laboratory’s Atmosphere Model version 4 (GFDL AM4) at three horizontal resolutions of 100 km, 50 km, and 25 km. The model produces more intense rainfall at finer resolutions, but a large discrepancy still exists between the simulated and the observed frequency distribution. We use a theoretical precipitation scaling diagnostic to examine the frequency distribution of the simulated rainfall. The scaling accurately produces the frequency distribution at moderate-to-high intensity ( $\geq 10 \text{ mm day}^{-1}$ ). Intense tropical rainfall at finer resolutions is produced primarily from the increased contribution of resolved precipitation and enhanced updrafts. The model becomes more sensitive to the grid-scale updrafts than local thermodynamics at high rain rates as the contribution from the resolved precipitation increases. On the contrary, the observed tropical precipitation extremes do not show a strong sensitivity to the grid-scale updrafts.

## Plain Language Summary

State of the art global scale climate models have horizontal resolutions of the order of tens of kilometers. However, these resolutions are much lower than the scales required to resolve tropical convection. This study investigates whether a resolution increase from 100 km to 25 km leads to any notable improvements in tropical rainfall simulation. Higher resolution simulations capture more intense rainfall events that are missed by their coarser counterparts. However, they struggle to capture the accurate frequency distribution of intense rainfall events. In addition, intense precipitation events in higher resolution simulations have different environmental conditions than the observed intense precipitation events. Results reported in this study underscore the importance of scrutinizing and carefully interpreting the outcomes of high-resolution climate model simulations.

## 1 Introduction

The representation of tropical rainfall is severely limited by the horizontal resolution of climate models, which is usually at the order of 100 km, whereas typical widths of upward motion in mature convective systems are in order of a few hundred meters to several kilometers (LeMone & Zipser, 1980; Matsuno, 2016). Convective systems interact with atmospheric circulation at various scales ranging from mesoscale to planetary-scale motions (Tomassini, 2020). Though many efforts have been made to count for the unresolved convection via the cumulus parameterization, these schemes are far from perfect and suffer large uncertainties. Therefore, increasing the resolution and improving cumulus parameterization remain the major focus areas of model development.

Though increasing horizontal resolution has model-dependent impacts, some common features are shared by a variety of general circulation models. They include increased contribution from the resolved precipitation, an intensified mean hydrological cycle and a higher frequency of precipitation extremes (Pope & Stratton, 2002; Demory et al., 2014; Hertwig et al., 2015; Terai et al., 2018; Herrington & Reed, 2020). Studies have also reported improved simulations of tropical and extratropical cyclones as the horizontal resolution increases (Zhao et al., 2009; Jung et al., 2012; Bacmeister et al., 2014; Demory et al., 2014). High-resolution ( $\sim 50 \text{ km}$ ) versions of the Geophysical Fluid Dynamics Laboratory’s (GFDL) general circulation model have shown significant improvements in simulations of tropical cyclones, atmospheric rivers, mesoscale convective systems and precipitation extremes (Zhao et al., 2009; Murakami et al., 2020; Zhao, 2020, 2022; Dong et al., 2023; Jong et al., 2023).

61 Finer scales of resolved motions and a better representation of orography in high  
62 resolution simulations are recognized to improve the representation of precipitation ex-  
63 tremes. Studies show that stronger vertical motions result in strengthening of precip-  
64 itation (eg., Terai et al. (2018); Herrington and Reed (2020)). However, a recent study  
65 using aquaplanet simulations at resolutions ranging from 50 km to 6 km (Lin et al., 2022)  
66 show that increasing vertical motion do not fully explain the changes in precipitation in-  
67 tensity in high resolution simulations. Donner et al. (2016) highlight the need to assess  
68 the influence of vertical motions in examining the impacts of changing resolution and  
69 simulating convection in the models. Precipitation extremes over land, the global mean  
70 precipitation rates, their patterns and evaporation rate do not always show consistent  
71 improvement as the model resolution increases (Bador et al., 2020; Pope & Stratton, 2002;  
72 Hourdin et al., 2013; Bacmeister et al., 2014; Hertwig et al., 2015). Therefore, it is es-  
73 sential to develop a process-based understanding of how increasing resolution changes  
74 the simulation of rainfall. In the present work, we use GFDL’s AM4 model to examine  
75 tropical rainfall distribution for three different resolutions viz., 100 km, 50 km and 25  
76 km. We assess the frequency distribution of rainfall rates using the theoretical precip-  
77 itation scaling diagnostic proposed by O’Gorman and Schneider (2009).

## 78 2 Data and methods

79 We use the GFDL atmospheric model version 4 (AM4) (Zhao et al., 2018a, 2018b)  
80 at three horizontal resolutions. The default GFDL AM4 utilizes a cubed-sphere topol-  
81 ogy for the atmospheric dynamical core with  $96 \times 96$  grid boxes (c96) per cube face re-  
82 sulting in a horizontal resolution of  $\sim 100$  km. Here, we use two additional high resolu-  
83 tion AM4 versions with  $192 \times 192$  (c192) and  $384 \times 384$  (c384) grid boxes per cube face,  
84 corresponding to horizontal resolutions of  $\sim 50$  km and  $\sim 25$  km, respectively. The de-  
85 fault GFDL AM4.0 (Zhao et al., 2018a, 2018b) serves as the atmospheric component of  
86 GFDL’s physical climate model (CM4, Held et al. (2019)), which participated in phase  
87 6 of the Coupled Model Intercomparison Project (CMIP6, Eyring et al. (2016)). c192AM4  
88 (Zhao, 2020) participated in the CMIP6 High Resolution Model Intercomparison Project  
89 (HighResMIP, Haarsma et al. (2016)). All three resolutions share the same atmospheric  
90 parameter setting as c192AM4 to remove uncertainties due to tuning. The parameter  
91 setting is documented in Zhao (2020). The default AM4 model’s performance is reported  
92 in Zhao et al. (2018a) and Zhao et al. (2018b). The performance of c192AM4 in simu-  
93 lating the mean precipitation and precipitation extremes is documented in detail in Zhao  
94 (2020) and Zhao (2022).

95 The global mean precipitation in three different resolutions viz., c96, c192, and c384  
96 are  $2.92 \text{ mm day}^{-1}$ ,  $2.96 \text{ mm day}^{-1}$ , and  $2.99 \text{ mm day}^{-1}$ , respectively for the period 1980-  
97 2000. The global mean precipitation increases progressively as the horizontal resolution  
98 of the model increases. Earlier studies (Duffy et al., 2003; Terai et al., 2018; Herrington  
99 & Reed, 2020) have noted a similar effect of horizontal resolution on simulated precip-  
100 itation. These values are higher than the observed global mean precipitation of  $2.67 \text{ mm}$   
101  $\text{day}^{-1}$  obtained using the the Global Precipitation Climatology Project (GPCP) dataset  
102 one degree daily dataset (1DD) Version 1.3 (Huffman et al., 2001) over the same period.  
103 Disagreement in the net longwave and shortwave fluxes at the surface (Supplementary  
104 Table 1) compared to observations (Trenberth et al., 2009) hint towards the differences  
105 in the mean simulated precipitation than the observed values. However, it is also impor-  
106 tant to note that the reliability of the GPCP dataset has been controversial (Gehne et  
107 al., 2016) and the radiative fluxes at the surface in the model lie within the range of dif-  
108 ferent observational estimates (Trenberth et al., 2009; Stephens et al., 2012; Wild et al.,  
109 2015; L’Ecuyer et al., 2015). The excessive precipitation in the Western Pacific near the  
110 Philippines (also known as the “Philippines hotspot” bias) and the dry biases over the  
111 eastern Atlantic and the Indian Ocean for c96 (Supplementary Fig. 1a) are reduced in  
112 c192 and c384 (Supplementary Fig. 1 b,c). However, the maritime continents (Supple-

113 elementary Fig. 1 b,c) and the eastern Pacific Inter Tropical Convergence Zone (ITCZ) move  
 114 towards a wetter bias as the resolution increases. Tuning the model could improve some  
 115 of the flux biases and thereby the mean precipitation biases. Zhao et al. (2018b) has in-  
 116 vestigated the effect of tuning on GFDL’s AM4 precipitation in detail.

117 The model runs are analyzed for the historical period (1980-2000) at the daily fre-  
 118 quency. We use daily precipitation dataset from the Tropical rainfall measurement mis-  
 119 sion (TRMM) version 3B42 (Huffman et al., 2007) and GPCP (Huffman et al., 2001) to  
 120 compare the model performance with observations. The comparison of the model runs  
 121 with observations are done for a common period of 1998-2000 over the tropics (30°S-30°N).  
 122 In addition, we use the daily mean of the European Centre for Medium-Range Weather  
 123 Forecasts (ECMWF) Reanalysis v5 (ERA5) (Hersbach et al., 2020) data at a horizon-  
 124 tal resolution of  $1^\circ \times 1^\circ$  for tropospheric temperature and winds. All model and obser-  
 125 vational variables are regridded to  $1^\circ \times 1^\circ$  horizontal resolution using conservative remap-  
 126 ping algorithm (python-cdo, (Schulzweida, 2022)). Histograms are normalized by a to-  
 127 tal number of data points that includes both rainy and non-rainy days.

## 128 3 Results

### 129 3.1 Rainfall intensity and frequency distribution

130 Figure 1 shows the normalized histogram of total daily precipitation intensity from  
 131 the model at three resolutions (c96, c192, and c384) and observations (TRMM and GPCP).  
 132 The normalized histogram (Fig. 1a) shows the most frequent nonzero rain rate. The sim-  
 133 ulated tropical rainfall peaks at  $\sim 1 \text{ mm day}^{-1}$ . On the other hand, GPCP has a peak  
 134 near  $\sim 10\text{-}15 \text{ mm day}^{-1}$ . All three resolutions produce more frequent rainfall than ob-  
 135 servations at lower rainrates ( $\leq 10 \text{ mm day}^{-1}$ ). This *too frequent too light* precipitation  
 136 bias (also known as drizzle bias) is a shared problem in the most general circulation mod-  
 137 els (Sun et al., 2006; Wilcox & Donner, 2007; Stephens et al., 2010; Pendergrass & Hart-  
 138 mann, 2014). It is also important to note that the observations suffer from the under-  
 139 estimation of light rainfall (Behrangi et al., 2012). TRMM has a broad frequency dis-  
 140 tribution without any clear peak. Precipitation radar aboard TRMM has a minimum  
 141 detectable signal of 17 dBz, making it poorly suited for detection of light rainfall (Behrangi  
 142 et al., 2012; Kummerow et al., 1998). The discrepancy in the frequency of light rainfall  
 143 is therefore partly attributed to the observational uncertainty.

144 The impact of horizontal resolution is evident at moderate rainfall rates. Interest-  
 145 ingly, c384 has a notable reduction in the frequency near the secondary peak for c96 and  
 146 c192 ( $\sim 3\text{-}10 \text{ mm day}^{-1}$ ). The bimodal frequency distribution of rainfall in c96 and  
 147 c192 becomes monomodal in c384. The removal of a secondary peak in c384 is mainly  
 148 due to the reduction in parameterized rainfall in c384 at these rainrates (Fig. 1c). All  
 149 three resolutions produce less frequent rainfall at moderate rainfall rates ( $20\text{-}40 \text{ mm}$   
 150  $\text{day}^{-1}$ ) compared to observations. On the contrary, the frequency of heavy rainfall ( $\geq$   
 151  $100 \text{ mm day}^{-1}$ ) is overestimated compared to GPCP in all three resolutions. The fre-  
 152 quency of high precipitation events in the model is closer to TRMM than GPCP. The  
 153 retrieved precipitation in TRMM is shown to be more reliable than GPCP at higher rain  
 154 rates (Behrangi et al., 2012). The frequency of heavy rainfall in c384 and c192 is over-  
 155 estimated compared to TRMM, whereas it is underestimated in c96.

156 The normalized histogram with a linear rainfall intensity scale (Fig. 1b) highlights  
 157 the upper tail of rainfall distribution. The model produces progressively more frequent  
 158 high rainfall events as the resolution increases. A few rare events with very high inten-  
 159 sity ( $\geq 300 \text{ mm day}^{-1}$ ) are captured by c384 and c192 but not by c96. The observed  
 160 precipitation tail goes up to  $1000 \text{ mm day}^{-1}$ , which is not captured by either resolution.  
 161 On the contrary, it is also important to note that the frequency of high precipitation events  
 162 ( $\sim 200\text{-}400 \text{ mm day}^{-1}$ ) is overestimated in high resolution simulations (c192 and c384)

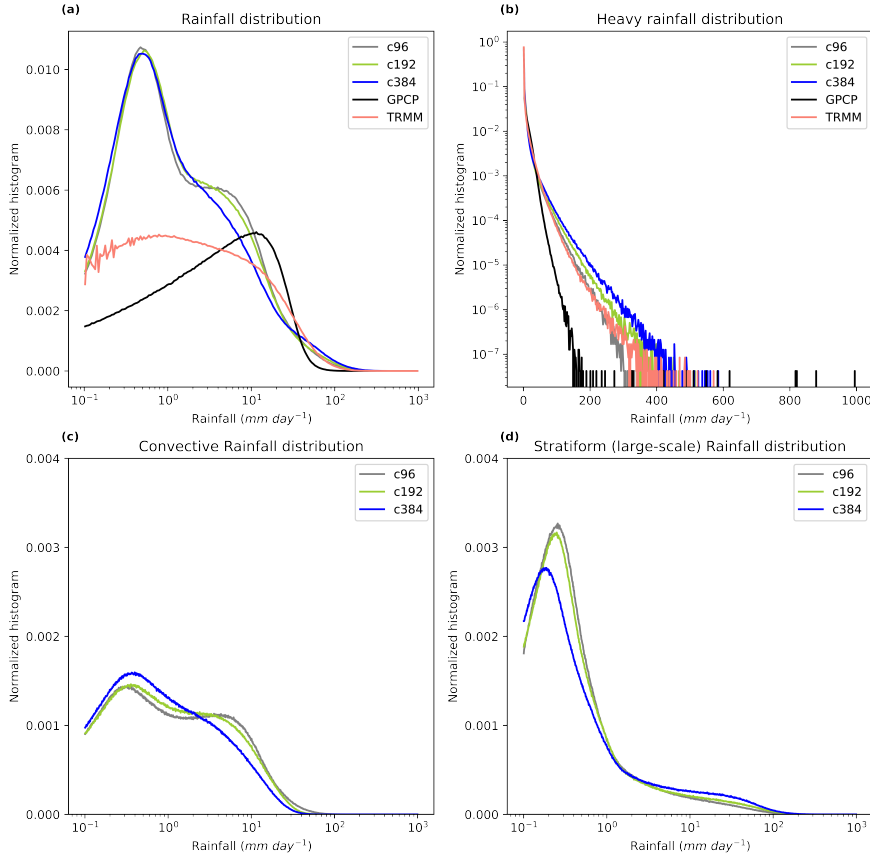


**Figure 1.** Normalized histogram of the daily mean rainfall (a) over logarithmic-scaled bins (rainfall intensity in  $mm\ day^{-1}$ ), (b) over a linear-scaled bins (rainfall intensity) and a logarithmic scale for y-axis (normalized histogram) to highlight the upper end of the distribution. Normalized histogram for (c) convective rainfall, (d) resolved/large-scale rainfall. The simulated (c96, c192, c384) and observed (TRMM and GPCP) precipitation datasets are regridded to  $1^\circ \times 1^\circ$  horizontal resolution using conservative remapping algorithm. Histograms are normalized by a total count of datapoints considering both rainy and nonrainy days. The figure is plotted for an overlap period of 1998-2000 for the model runs and observations over the tropics ( $30^\circ\text{S}$ - $30^\circ\text{N}$ ).

163 compared to the observations. This analysis shows that the model produces intense tropical  
 164 rainfall with the increasing horizontal resolution, but it overestimates the frequency  
 165 of precipitation extremes.

### 166 3.2 Factors affecting the rainfall intensity distribution

167 Increasing the horizontal resolution changes the partitioning between precipitation  
 168 produced by the convection scheme (parameterized precipitation, *prec\_conv*) and the large-  
 169 scale scheme (resolved precipitation, *prec\_ls*). The contribution of resolved precipitation  
 170 to the mean precipitation in the tropics increases from about 30% in c96 to more than  
 171 50% in c384 (Supplementary Fig. 2). The normalized frequency distribution for convec-  
 172 tive rainfall shifts towards lower intensity as the horizontal resolution increases (Fig. 1c).  
 173 It is indicated by a progressively higher peak of normalized histogram at low convective

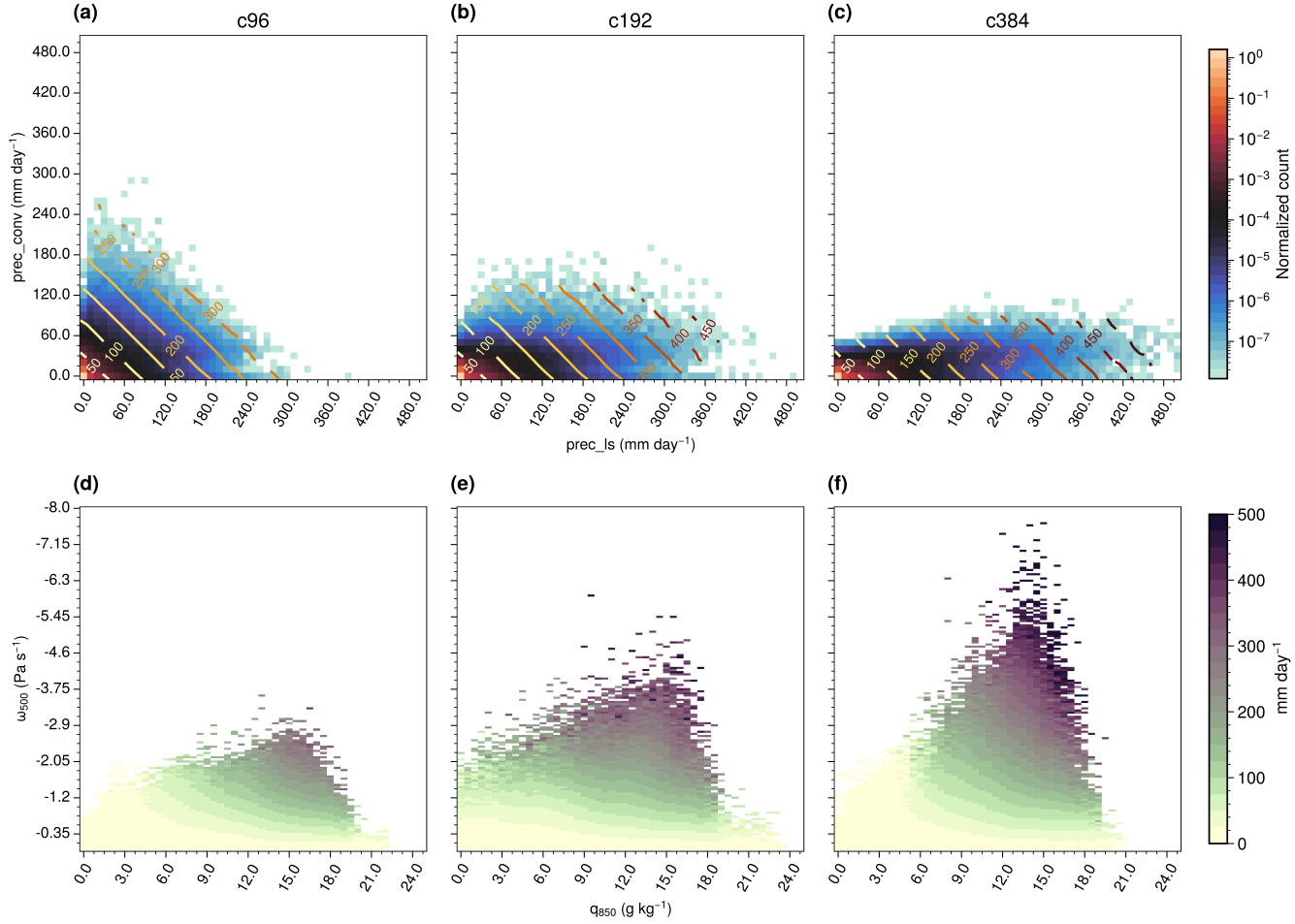


**Figure 2.** (a) 2D bin mean of normalized count (shading) and mean precipitation intensity (in  $mm\ day^{-1}$  indicated by contours) as a function of convective (prec\_conv) and large-scale (prec\_ls) rainfall. (b) 2D bin mean precipitation intensity ( $mm\ day^{-1}$ ) as a function of low-level moisture ( $q_{850}$ ) and mid-tropospheric pressure velocity ( $\omega_{500}$ ). The figure is plotted for model simulations over a historical period of 1980-2000.

174 rainfall rates ( $\leq 2\ mm\ day^{-1}$ ) and a reduction in the frequency at higher rainrates as the  
 175 horizontal resolution increases (Fig. 1c). On the other hand, the frequency of large-scale  
 176 rainfall exhibit a reduction in the peak at low rainfall rates and an increase at high rain  
 177 rates for high resolution runs (Fig. 1d). This shows that the large-scale scheme progres-  
 178 sively does more work at high rainfall intensities as the horizontal resolution increases.  
 179 Figure 2 a-c shows the joint distribution of the resolved and the parameterized precipi-  
 180 tation. The shading represents the 2D bin mean normalized count and the contours show  
 181 the mean precipitation intensity. The count is normalized by a total number of datapoints  
 182 considering both rainy and non-rainy days. For c96, both parameterized and large-scale  
 183 schemes contribute almost equally at all precipitation intensities. However, the parti-  
 184 tioning between parameterized and resolved precipitation changes in c192 and c384. In-  
 185 tense rainfall in c192 and c384 comes mainly from the large-scale scheme. Convective  
 186 rainfall in c96 contributes up to a maximum intensity of  $300\ mm\ day^{-1}$ . However, it de-

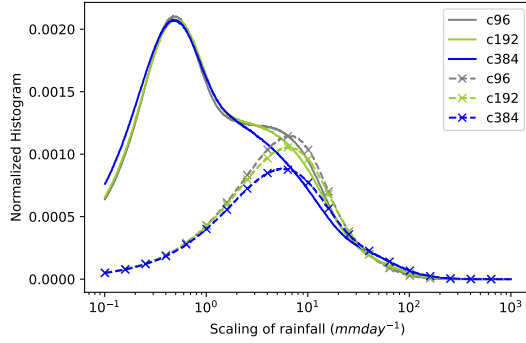


**Figure 3.** Normalized histogram of the model simulated mean daily rainfall (solid lines) and rainfall obtained from the theoretical precipitation scaling (marked-dotted lines) using equation (1). The histograms are plotted for the model runs over a historical period of 1980-2000.

187 creases below  $200 \text{ mm day}^{-1}$  in c192 and it decreases even further in c384 (below  $120$   
188  $\text{mm day}^{-1}$ ).

189 Two important ingredients to understand the rainfall intensity distribution are mois-  
190 ture and updraft velocity. We look at the 2D distribution of precipitation intensity as  
191 a function of low level moisture ( $q_{850}$ ) and mid-tropospheric updraft velocity ( $\omega_{500}$ ) for  
192 three different resolutions (Fig. 2). As expected, rainfall intensity increases as moisture  
193 content and vertical velocity increase. The range of moisture content in three resolutions  
194 is not much different, however, the maximum vertical velocity increases by a factor of  
195  $\sim 1.7$  from c96 to c192, and about  $\sim 2.3$  from c96 to c384. Intense rainfall at finer res-  
196 olutions mainly occurs at high updraft velocity (Fig. 2 e, f). In addition, the sensitiv-  
197 ity of the precipitation intensity to high updraft velocity is contributed mainly by the  
198 resolved precipitation (Supplementary Fig. 3). In all three resolutions, large-scale pre-  
199 cipitation shows a more sensitivity to updrafts than moisture (Supplementary Fig. 3 d-  
200 f). The parameterized precipitation instead shows sensitivity to low-level moisture un-  
201 like the resolved precipitation (Supplementary Fig. 3 a-c). Qualitative similarities be-  
202 tween the total rainfall intensity distribution (Fig. 2 d-f) and the resolved precipitation  
203 (Supplementary Fig. 3 d-f) suggests that the sensitivity of precipitation intensity to the  
204 updraft velocity at high rainrates comes primarily from the resolved precipitation. This  
205 analysis indicates that as the horizontal resolution increases, the increase in rainfall in-  
206 tensity is associated primarily with the enhanced updraft velocity rather than the mois-  
207 ture content, and these changes come mainly from resolved (large-scale) precipitation.

### 208 3.3 Precipitation scaling

209 To further understand the impact of horizontal resolution on the rainfall frequency  
210 distribution, we use the precipitation scaling diagnostic proposed by O’Gorman and Schnei-  
211 der (2009). This diagnostic has been used primarily to study the changes in precipita-  
212 tion extremes with warming (O’Gorman, 2012; Singh & O’Gorman, 2014; Pfahl et al.,  
213 2017; Nie et al., 2018). The scaling is given by

$$P \approx - \left\{ \omega \frac{\partial q_s}{\partial p} \Big|_{\theta^*} \right\} \quad (1)$$

214 where precipitation intensity ( $P$ ) is calculated from a column integrated product of pres-  
215 sure velocity ( $\omega$ ) and the vertical derivative of saturation specific humidity taken along  
216 a moist adiabat profile ( $\frac{\partial q_s}{\partial p} \Big|_{\theta^*}$ ). The right hand side of the equation (1) corresponds to  
217 the column integrated condensation rate. The condensation maintains saturation of the

218 rising air parcel. This scaling assumes that precipitation efficiency is  $\sim 1$  and all of the  
 219 condensed water vapor falls as rainfall. The diabatic effects other than latent heating  
 220 are neglected ( $\theta^*$  is conserved; shown by Muller et al. (2011)). This scaling is expected  
 221 to work better at higher precipitation intensities when air parcels are nearly saturated.  
 222 However, we test it at all intensities.

223 The scaling captures the spatial distribution of deep convective areas of the tropics  
 224 quite well, but it underestimates the intensity of the mean rainfall (Supplementary  
 225 Fig. 4). Despite the assumptions mentioned earlier, the scaling captures the frequency  
 226 distribution of rainfall at moderate to high intensity remarkably well in all three reso-  
 227 lutions (Fig. 3 a). The scaling does not capture the model drizzle. We will discuss the  
 228 possible reasons for it shortly. The frequency distribution of rainfall obtained by the scal-  
 229 ing is monomodal. It peaks near  $5\text{-}8 \text{ mm day}^{-1}$  for all three resolutions, which is close  
 230 to the secondary peak of rainfall frequency distribution in c96 and c192. The scaling ac-  
 231 curately produces this peak and captures the increasing magnitude from c384 to c96. Af-  
 232 ter this peak, the precipitation scaling closely follows the frequency of simulated precipi-  
 233 tation in all three resolutions. At moderate and high rainfall intensities, it overestimates  
 234 the frequency of model simulated precipitation. However, the scaling captures the over-  
 235 all shape at high rain rates, including a peak in c384 near  $50 \text{ mm day}^{-1}$ .

236 As the contribution from radiative fluxes other than latent heat is non-negligible  
 237 ( $\theta^*$  is not conserved) at low rainfall intensity, the scaling is not expected to work at low  
 238 rain rates. In addition, the model drizzle mainly comes from the subsaturated regions  
 239 ( $q \ll q_s$ ) (Terai et al., 2016). Earlier work suggests that a crude representation of pa-  
 240 rameterized convection could be the cause of drizzle bias in the models (Suzuki et al.,  
 241 2013; Stephens et al., 2010). As we use grid-scale (resolved) variables to estimate the pre-  
 242 cipitation scaling, it can not capture subgrid scale convective processes. The above rea-  
 243 sons possibly explain why precipitation scaling does not reproduce an accurate frequency  
 244 of the model drizzle. In addition, the above scaling formulation does not include precipi-  
 245 tation efficiency. The large-scale precipitation efficiency is affected by several factors such  
 246 as mid level moisture, Convective available potential energy (CAPE), convective organ-  
 247 ization and microphysical processes (Muller & Takayabu, 2020; Zhao et al., 2016; Singh  
 248 & O’Gorman, 2014). The overestimation of high rain rates by the scaling is likely due  
 249 to the omission of precipitation efficiency in the calculations.

250 We plot the 2D bin mean of normalized precipitation intensity as a function of column-  
 251 integrated vertical velocity ( $\{\omega\}$ ) and the column-integrated vertical derivative of sat-  
 252 urated specific humidity ( $\left\{\frac{\partial q_s}{\partial p}\right\}_{\theta^*}$ ) (Fig. 4). As the maximum precipitation intensity  
 253 in simulations and observations vary over a large range (Fig. 1 b), we normalize precipi-  
 254 tation intensity by the maximum 2D bin mean value for each dataset. The precipita-  
 255 tion intensity distribution without normalizing has similar features (Supplementary Fig.  
 256 5). The increase in precipitation intensity at higher resolution comes mainly from the  
 257 changes in updraft velocity rather than changes in thermal stratification ( $\left\{\frac{\partial q_s}{\partial p}\right\}_{\theta^*}$ ) as  
 258 the horizontal resolution increases (Fig. 4 a-c). Intense precipitation events in the model  
 259 are strongly tied to the grid-scale updrafts unlike observations (Fig. 4 e-f). We see that  
 260 observed heavy precipitation events can occur even at moderate updrafts if the thermal  
 261 stratification (Fig. 4 e-f, Supplementary Fig. 5 e-f) or low-level moisture (Supplemen-  
 262 tary Fig. 6 e-f) is high. Interestingly, ERA5 precipitation is also tied to stronger grid-  
 263 scale updrafts but relatively to a lesser extent than GFDL’s AM4 model. In c384, the  
 264 grid-scale updrafts are much more intense than the reanalysis updrafts. The maximum  
 265 grid-scale updraft at 500 hPa in c384 is about two times the maximum grid-scale updraft  
 266 in ERA5 (Supplementary Fig. 6). It should be noted that the updrafts in reanalysis datasets  
 267 suffer from uncertainties (Uma et al., 2021). Nonetheless, observational studies have noted  
 268 the importance of local thermodynamics for tropical rainfall and the onset of precipi-  
 269 tation (Houze Jr, 1989; Bretherton et al., 2004; Neelin et al., 2022). A typical size of up-  
 270 drafts in tropical convective systems is in order of a few kilometers (LeMone & Zipser,

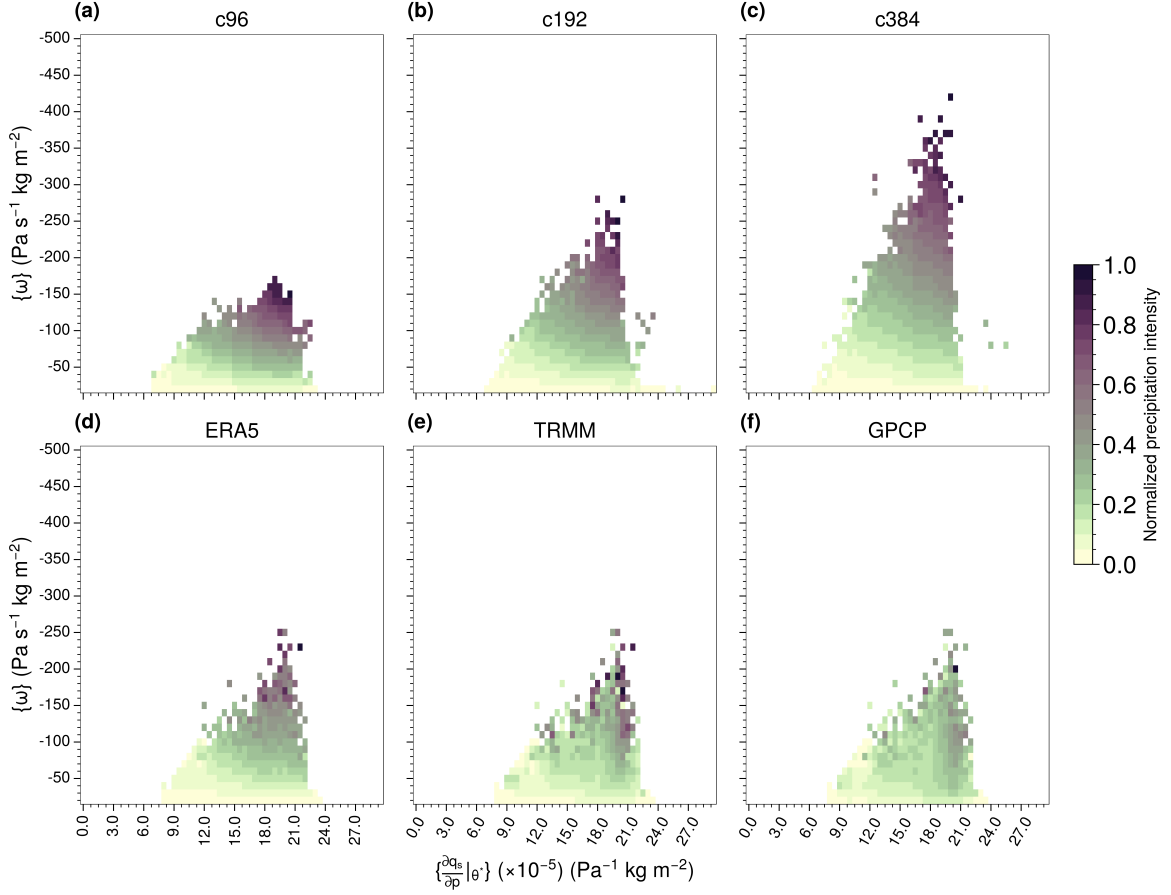


**Figure 4.** 2D bin mean of normalized precipitation intensity as a function of column-integrated pressure velocity  $\{\omega\}$  and the column-integrated vertical derivative of saturated specific humidity along the moist adiabat  $\left\{\frac{\partial q_s}{\partial p}\right\}_{\theta^*}$ . Precipitation intensity (in  $mm\ day^{-1}$ ) is normalized by maximum 2D bin value for each subplot. The figure is plotted using the data for an overlap period of 1998-2000.

271 1980; Matsuno, 2016), we would expect the cancellation of updrafts and downdrafts when  
 272 averaged over an area of  $\sim 1^\circ \times 1^\circ$ . In turn, we expect to see a less dependence of grid-  
 273 scale updrafts for observed precipitation extremes.

274 Intense precipitation in c384 and c192 are closely tied to strong updrafts. The sensi-  
 275 tivity of the simulated precipitation to the grid-scale updraft velocity mainly comes from  
 276 the resolved precipitation and not from the parameterized precipitation (Supplementary  
 277 Fig. 3). In this regard, tropical precipitation extremes in high resolution simulations ex-  
 278 hibit similarities to grid-scale storms (Held et al., 2007). This suggests that even though  
 279 the model is able to capture high intensity events as the horizontal resolution increases,  
 280 with the increased contribution from the resolved precipitation, it comes at the expense  
 281 of the model being overly sensitive to the grid-scale updraft velocity.

## 4 Discussion

We examine the distribution of tropical rainfall using GFDL’s AM4 model at three horizontal resolutions viz., c96 ( $\sim 100$  km), c192 ( $\sim 50$  km) and c384 ( $\sim 25$  km). As the horizontal resolution increases, we observe a progressive increase in the upper percentile of rainfall (precipitation extremes), increased contribution from the resolved precipitation and enhanced vertical velocities. These features are similar to earlier studies using different general circulation models (eg., Terai et al. (2018); Herrington and Reed (2020)). The model overestimates the frequency of light rainfall (drizzle bias) and underestimates the moderate rainfall in all three simulations. At finer resolutions (c192 and c384), the model produces more intense rainfall, but it overestimates the frequency of occurrence of heavy rainfall events compared to observed datasets (Fig. 1). The increase in precipitation extremes at high resolution is primarily contributed by the resolved precipitation and mainly comes from enhanced updrafts (Fig. 2).

We use theoretical precipitation scaling proposed by O’Gorman and Schneider (2009) to assess the frequency distribution of tropical rainfall. The scaling utilizes the grid-scale vertical velocity and temperature profiles to estimate an approximate precipitation intensity. Despite this simple formulation, the scaling produces the frequency distribution of model simulated precipitation remarkably well at moderate to high rain rates (Figure 3). Earlier studies have used the scaling to examine changes in precipitation extremes (O’Gorman, 2012; Singh & O’Gorman, 2014; Pfahl et al., 2017; Nie et al., 2018). In the GFDL model, the scaling reproduces the frequency distribution of tropical rainfall even at moderate rainfall rates ( $\geq 10$  mm day<sup>-1</sup>). This could be a model dependent result, but it would be interesting to check the scaling for the other general circulation models.

Precipitation extremes in the model are closely tied to the grid-scale intense updrafts and relatively less sensitive to thermal stratification (Figure 4 a-c) and low-level moisture (Supplementary Fig. 6 a-c). In observed datasets, however, intense precipitation events can occur at moderate updraft velocities if thermal stratification (Figure 4 e-f) and low-level moisture are high (Supplementary Fig. 6 e-f). This high sensitivity of the model to updrafts comes mainly from the resolved precipitation (Supplementary Fig. 3). Convective precipitation shows sensitivity to local thermodynamics mimicking the observed tropical precipitation behavior closely (Bretherton et al., 2004; Neelin et al., 2022). On the other hand, resolved precipitation has been shown to capture geographical patterns and rain rates (Kooperman et al., 2018) better than parameterized precipitation. Convective precipitation also struggles to capture the accurate diurnal cycle of precipitation (Zhao et al., 2018a). This study suggests that the amount of rainfall obtained from the resolved precipitation and its sensitivity to the grid-scale vertical motion should be examined carefully at least until the updrafts and downdrafts in convective systems are resolved explicitly. We reiterate the suggestion by Donner et al. (2016) on the importance of recognizing the dependence of resolved vertical velocity on resolution and utilizing it to understand the impacts of resolution realistically. Our results suggest that additional process-based evaluation is necessary to assess the performance of both parameterized and resolved precipitation.

## References

- Bacmeister, J. T., Wehner, M. F., Neale, R. B., Gettelman, A., Hannay, C., Lauritzen, P. H., . . . Truesdale, J. E. (2014). Exploratory high-resolution climate simulations using the community atmosphere model (cam). *Journal of Climate*, 27(9), 3073–3099.
- Bador, M., Boé, J., Terray, L., Alexander, L. V., Baker, A., Bellucci, A., . . . others (2020). Impact of higher spatial atmospheric resolution on precipitation extremes over land in global climate models. *Journal of Geophysical Research:*

- 333 *Atmospheres*, 125(13), e2019JD032184.
- 334 Behrangi, A., Lebsock, M., Wong, S., & Lambigtsen, B. (2012). On the quantifi-  
 335 cation of oceanic rainfall using spaceborne sensors. *Journal of Geophysical Re-*  
 336 *search: Atmospheres*, 117(D20).
- 337 Bretherton, C. S., Peters, M. E., & Back, L. E. (2004). Relationships between wa-  
 338 ter vapor path and precipitation over the tropical oceans. *Journal of climate*,  
 339 17(7), 1517–1528.
- 340 Demory, M.-E., Vidale, P. L., Roberts, M. J., Berrisford, P., Strachan, J., Schie-  
 341 mann, R., & Mizielinski, M. S. (2014). The role of horizontal resolution in  
 342 simulating drivers of the global hydrological cycle. *Climate dynamics*, 42,  
 343 2201–2225.
- 344 Dong, W., Zhao, M., Ming, Y., Krasting, J. P., & Ramaswamy, V. (2023). Sim-  
 345 ulation of united states mesoscale convective systems using gfdl’s new high-  
 346 resolution general circulation model. *Journal of Climate*, 1–40.
- 347 Donner, L. J., O’Brien, T. A., Rieger, D., Vogel, B., & Cooke, W. F. (2016). Are at-  
 348 mospheric updrafts a key to unlocking climate forcing and sensitivity? *Atmo-*  
 349 *spheric Chemistry and Physics*, 16(20), 12983–12992.
- 350 Duffy, P., Govindasamy, B., Iorio, J., Milovich, J., Sperber, K., Taylor, K., ...  
 351 Thompson, S. (2003). High-resolution simulations of global climate, part  
 352 1: present climate. *Climate Dynamics*, 21, 371–390.
- 353 Eyring, V., Bony, S., Meehl, G. A., Senior, C. A., Stevens, B., Stouffer, R. J., &  
 354 Taylor, K. E. (2016). Overview of the coupled model intercomparison project  
 355 phase 6 (cmip6) experimental design and organization. *Geoscientific Model*  
 356 *Development*, 9(5), 1937–1958.
- 357 Gehne, M., Hamill, T. M., Kiladis, G. N., & Trenberth, K. E. (2016). Comparison  
 358 of global precipitation estimates across a range of temporal and spatial scales.  
 359 *Journal of Climate*, 29(21), 7773–7795.
- 360 Haarsma, R. J., Roberts, M. J., Vidale, P. L., Senior, C. A., Bellucci, A., Bao, Q.,  
 361 ... others (2016). High resolution model intercomparison project (highresmip  
 362 v1.0) for cmip6. *Geoscientific Model Development*, 9(11), 4185–4208.
- 363 Held, I. M., Guo, H., Adcroft, A., Dunne, J., Horowitz, L., Krasting, J., ... others  
 364 (2019). Structure and performance of gfdl’s cm4.0 climate model. *Journal of*  
 365 *Advances in Modeling Earth Systems*, 11(11), 3691–3727.
- 366 Held, I. M., Zhao, M., & Wyman, B. (2007). Dynamic radiative–convective equilib-  
 367 ria using gcm column physics. *Journal of the atmospheric sciences*, 64(1), 228–  
 368 238.
- 369 Herrington, A. R., & Reed, K. A. (2020). On resolution sensitivity in the commu-  
 370 nity atmosphere model. *Quarterly Journal of the Royal Meteorological Society*,  
 371 146(733), 3789–3807.
- 372 Hersbach, H., Bell, B., Berrisford, P., Hirahara, S., Horányi, A., Muñoz-Sabater, J.,  
 373 ... others (2020). The era5 global reanalysis. *Quarterly Journal of the Royal*  
 374 *Meteorological Society*, 146(730), 1999–2049.
- 375 Hertwig, E., von Storch, J.-S., Handorf, D., Dethloff, K., Fast, I., & Krismer, T.  
 376 (2015). Effect of horizontal resolution on echam6-amip performance. *Climate*  
 377 *Dynamics*, 45, 185–211.
- 378 Hourdin, F., Foujols, M.-A., Codron, F., Guemas, V., Dufresne, J.-L., Bony, S., ...  
 379 others (2013). Impact of the lmdz atmospheric grid configuration on the cli-  
 380 mate and sensitivity of the ipsl-cm5a coupled model. *Climate Dynamics*, 40,  
 381 2167–2192.
- 382 Houze Jr, R. A. (1989). Observed structure of mesoscale convective systems and im-  
 383 plications for large-scale heating. *Quarterly Journal of the Royal Meteorological*  
 384 *Society*, 115(487), 425–461.
- 385 Huffman, G. J., Adler, R. F., Morrissey, M. M., Bolvin, D. T., Curtis, S., Joyce, R.,  
 386 ... Susskind, J. (2001). Global precipitation at one-degree daily resolution  
 387 from multisatellite observations. *Journal of hydrometeorology*, 2(1), 36–50.

- 388 Huffman, G. J., Bolvin, D. T., Nelkin, E. J., Wolff, D. B., Adler, R. F., Gu, G., ...  
 389 Stocker, E. F. (2007). The trmm multisatellite precipitation analysis (tmpa):  
 390 Quasi-global, multiyear, combined-sensor precipitation estimates at fine scales.  
 391 *Journal of hydrometeorology*, *8*(1), 38–55.
- 392 Jong, B.-T., Delworth, T. L., Cooke, W. F., Tseng, K.-C., & Murakami, H. (2023).  
 393 Increases in extreme precipitation over the northeast united states using high-  
 394 resolution climate model simulations. *npj Climate and Atmospheric Science*,  
 395 *6*(1), 18.
- 396 Jung, T., Miller, M., Palmer, T., Towers, P., Wedi, N., Achuthavarier, D., ... oth-  
 397 ers (2012). High-resolution global climate simulations with the ecmwf model  
 398 in project athena: Experimental design, model climate, and seasonal forecast  
 399 skill. *Journal of Climate*, *25*(9), 3155–3172.
- 400 Kooperman, G. J., Pritchard, M. S., O'Brien, T. A., & Timmermans, B. W. (2018).  
 401 Rainfall from resolved rather than parameterized processes better represents  
 402 the present-day and climate change response of moderate rates in the commu-  
 403 nity atmosphere model. *Journal of advances in modeling earth systems*, *10*(4),  
 404 971–988.
- 405 Kummerow, C., Barnes, W., Kozu, T., Shiue, J., & Simpson, J. (1998). The tropical  
 406 rainfall measuring mission (trmm) sensor package. *Journal of atmospheric and*  
 407 *oceanic technology*, *15*(3), 809–817.
- 408 LeMone, M. A., & Zipser, E. J. (1980). Cumulonimbus vertical velocity events  
 409 in gate. part i: Diameter, intensity and mass flux. *Journal of the Atmospheric*  
 410 *Sciences*, *37*(11), 2444–2457.
- 411 Lin, P., Ming, Y., & Robinson, T. (2022). On the resolution sensitivity in a gfdl  
 412 global atmospheric model. *Authorea Preprints*.
- 413 L'Ecuyer, T. S., Beaudoin, H., Rodell, M., Olson, W., Lin, B., Kato, S., ... oth-  
 414 ers (2015). The observed state of the energy budget in the early twenty-first  
 415 century. *Journal of Climate*, *28*(21), 8319–8346.
- 416 Matsuno, T. (2016). Prologue: tropical meteorology 1960–2010—personal recollec-  
 417 tions. *Meteorological Monographs*, *56*, vii–xv.
- 418 Muller, C., O'Gorman, P. A., & Back, L. E. (2011). Intensification of precipita-  
 419 tion extremes with warming in a cloud-resolving model. *Journal of Climate*,  
 420 *24*(11), 2784–2800.
- 421 Muller, C., & Takayabu, Y. (2020). Response of precipitation extremes to warming:  
 422 what have we learned from theory and idealized cloud-resolving simulations,  
 423 and what remains to be learned? *Environmental Research Letters*, *15*(3),  
 424 035001.
- 425 Murakami, H., Delworth, T. L., Cooke, W. F., Zhao, M., Xiang, B., & Hsu, P.-C.  
 426 (2020). Detected climatic change in global distribution of tropical cyclones.  
 427 *Proceedings of the National Academy of Sciences*, *117*(20), 10706–10714.
- 428 Neelin, J. D., Martinez-Villalobos, C., Stechmann, S. N., Ahmed, F., Chen, G., Nor-  
 429 ris, J. M., ... Lenderink, G. (2022). Precipitation extremes and water vapor:  
 430 Relationships in current climate and implications for climate change. *Current*  
 431 *Climate Change Reports*, *8*(1), 17–33.
- 432 Nie, J., Sobel, A. H., Shaevitz, D. A., & Wang, S. (2018). Dynamic amplification of  
 433 extreme precipitation sensitivity. *Proceedings of the National Academy of Sci-*  
 434 *ences*, *115*(38), 9467–9472.
- 435 Nikumbh, A., Lin, P., Paynter, D., & Ming, Y. (2023a, October). *Supporting data*  
 436 *1 for "Does increasing horizontal resolution improve the simulation of intense*  
 437 *tropical rainfall?"*. Zenodo. Retrieved from [https://doi.org/10.5281/](https://doi.org/10.5281/zenodo.8433128)  
 438 [zenodo.8433128](https://doi.org/10.5281/zenodo.8433128) doi: 10.5281/zenodo.8433128
- 439 Nikumbh, A., Lin, P., Paynter, D., & Ming, Y. (2023b, October). *Supporting data*  
 440 *2 for "Does increasing horizontal resolution improve the simulation of intense*  
 441 *tropical rainfall?"*. Zenodo. Retrieved from [https://doi.org/10.5281/](https://doi.org/10.5281/zenodo.8433235)  
 442 [zenodo.8433235](https://doi.org/10.5281/zenodo.8433235) doi: 10.5281/zenodo.8433235

- 443 Nikumbh, A., Lin, P., Paynter, D., & Ming, Y. (2023c, October). *Supporting data*  
 444 *3 for "Does increasing horizontal resolution improve the simulation of intense*  
 445 *tropical rainfall?"*. Zenodo. Retrieved from [https://doi.org/10.5281/](https://doi.org/10.5281/zenodo.8433237)  
 446 [zenodo.8433237](https://doi.org/10.5281/zenodo.8433237) doi: 10.5281/zenodo.8433237
- 447 O’Gorman, P. A. (2012). Sensitivity of tropical precipitation extremes to climate  
 448 change. *Nature Geoscience*, *5*(10), 697–700.
- 449 O’Gorman, P. A., & Schneider, T. (2009). Scaling of precipitation extremes over  
 450 a wide range of climates simulated with an idealized gcm. *Journal of Climate*,  
 451 *22*(21), 5676–5685.
- 452 Pendergrass, A. G., & Hartmann, D. L. (2014). Changes in the distribution of rain  
 453 frequency and intensity in response to global warming. *Journal of Climate*,  
 454 *27*(22), 8372–8383.
- 455 Pfahl, S., O’Gorman, P. A., & Fischer, E. M. (2017). Understanding the regional  
 456 pattern of projected future changes in extreme precipitation. *Nature Climate*  
 457 *Change*, *7*(6), 423–427.
- 458 Pope, V., & Stratton, R. (2002). The processes governing horizontal resolution sensi-  
 459 tivity in a climate model. *Climate Dynamics*, *19*, 211–236.
- 460 Schulzweida, U. (2022, October). *Cdo user guide*. Zenodo. Retrieved from [https://](https://doi.org/10.5281/zenodo.7112925)  
 461 [doi.org/10.5281/zenodo.7112925](https://doi.org/10.5281/zenodo.7112925) doi: 10.5281/zenodo.7112925
- 462 Singh, M. S., & O’Gorman, P. A. (2014). Influence of microphysics on the scal-  
 463 ing of precipitation extremes with temperature. *Geophysical Research Letters*,  
 464 *41*(16), 6037–6044.
- 465 Stephens, G. L., L’Ecuyer, T., Forbes, R., Gettelmen, A., Golaz, J.-C., Bodas-  
 466 Salcedo, A., ... Haynes, J. (2010). Dreary state of precipitation in global  
 467 models. *Journal of Geophysical Research: Atmospheres*, *115*(D24).
- 468 Stephens, G. L., Li, J., Wild, M., Clayson, C. A., Loeb, N., Kato, S., ... Andrews,  
 469 T. (2012). An update on earth’s energy balance in light of the latest global  
 470 observations. *Nature Geoscience*, *5*(10), 691–696.
- 471 Sun, Y., Solomon, S., Dai, A., & Portmann, R. W. (2006). How often does it rain?  
 472 *Journal of climate*, *19*(6), 916–934.
- 473 Suzuki, K., Golaz, J.-C., & Stephens, G. L. (2013). Evaluating cloud tuning in a cli-  
 474 mate model with satellite observations. *Geophysical Research Letters*, *40*(16),  
 475 4464–4468.
- 476 Terai, C. R., Caldwell, P., & Klein, S. A. (2016). Why do climate models drizzle  
 477 too much and what impact does this have. In *Agu fall meeting abstracts* (Vol.  
 478 2016, pp. A53K–01).
- 479 Terai, C. R., Caldwell, P. M., Klein, S. A., Tang, Q., & Branstetter, M. L. (2018).  
 480 The atmospheric hydrologic cycle in the acme v0. 3 model. *Climate Dynamics*,  
 481 *50*(9-10), 3251–3279.
- 482 Tomassini, L. (2020). The interaction between moist convection and the atmo-  
 483 spheric circulation in the tropics. *Bulletin of the American Meteorological Soci-*  
 484 *ety*, *101*(8), E1378–E1396.
- 485 Trenberth, K. E., Fasullo, J. T., & Kiehl, J. (2009). Earth’s global energy budget.  
 486 *Bulletin of the american meteorological society*, *90*(3), 311–324.
- 487 Uma, K. N., Das, S. S., Ratnam, M. V., & Suneeth, K. V. (2021). Assessment of  
 488 vertical air motion among reanalyses and qualitative comparison with very-  
 489 high-frequency radar measurements over two tropical stations. *Atmospheric*  
 490 *Chemistry and Physics*, *21*(3), 2083–2103.
- 491 Wilcox, E. M., & Donner, L. J. (2007). The frequency of extreme rain events in  
 492 satellite rain-rate estimates and an atmospheric general circulation model.  
 493 *Journal of Climate*, *20*(1), 53–69.
- 494 Wild, M., Folini, D., Hakuba, M. Z., Schär, C., Seneviratne, S. I., Kato, S., ...  
 495 König-Langlo, G. (2015). The energy balance over land and oceans: an as-  
 496 sessment based on direct observations and cmip5 climate models. *Climate*  
 497 *Dynamics*, *44*, 3393–3429.

- 498 Zhao, M. (2020). Simulations of atmospheric rivers, their variability, and response  
 499 to global warming using gfdl’s new high-resolution general circulation model.  
 500 *Journal of Climate*, *33*(23), 10287–10303.
- 501 Zhao, M. (2022). A study of ar-, ts-, and mcs-associated precipitation and extreme  
 502 precipitation in present and warmer climates. *Journal of Climate*, *35*(2), 479–  
 503 497.
- 504 Zhao, M., Golaz, J.-C., Held, I., Guo, H., Balaji, V., Benson, R., . . . others (2018a).  
 505 The gfdl global atmosphere and land model am4. 0/lm4. 0: 1. simulation  
 506 characteristics with prescribed ssts. *Journal of Advances in Modeling Earth  
 507 Systems*, *10*(3), 691–734.
- 508 Zhao, M., Golaz, J.-C., Held, I., Guo, H., Balaji, V., Benson, R., . . . others (2018b).  
 509 The gfdl global atmosphere and land model am4. 0/lm4. 0: 2. model descrip-  
 510 tion, sensitivity studies, and tuning strategies. *Journal of Advances in Model-  
 511 ing Earth Systems*, *10*(3), 735–769.
- 512 Zhao, M., Golaz, J.-C., Held, I. M., Ramaswamy, V., Lin, S.-J., Ming, Y., . . . others  
 513 (2016). Uncertainty in model climate sensitivity traced to representations of  
 514 cumulus precipitation microphysics. *Journal of Climate*, *29*(2), 543–560.
- 515 Zhao, M., Held, I. M., Lin, S.-J., & Vecchi, G. A. (2009). Simulations of global  
 516 hurricane climatology, interannual variability, and response to global warming  
 517 using a 50-km resolution gcm. *Journal of Climate*, *22*(24), 6653–6678.

## 518 Open Research Section

519 The AM4 model code is provided at [https://data1.gfdl.noaa.gov/nomads/forms/  
 520 am4.0/](https://data1.gfdl.noaa.gov/nomads/forms/am4.0/) (Zhao et al., 2018a, 2018b). The configuration of the simulations presented in  
 521 this manuscript is described in Zhao (2020). The model outputs used are available at:  
 522 <https://zenodo.org/record/8433128>, <https://zenodo.org/record/8433235> and [https://  
 523 zenodo.org/record/8433237](https://zenodo.org/record/8433237) (Nikumbh et al., 2023a, 2023b, 2023c). The ERA5 data  
 524 can be downloaded from [https://cds.climate.copernicus.eu/cdsapp#!/dataset/  
 525 reanalysis-era5-complete?tab=overview](https://cds.climate.copernicus.eu/cdsapp#!/dataset/reanalysis-era5-complete?tab=overview) (Hersbach et al., 2020). The GPCP pre-  
 526 cipitation dataset is available [https://rda.ucar.edu/datasets/ds728.7/dataaccess/  
 527 \(Huffman et al., 2001\). The TRMM precipitation data is downloaded from \[https://disc  
 528 .gsfc.nasa.gov/datasets?keywords=TRMM\\\_3B42.7&page=1\]\(https://disc.gsfc.nasa.gov/datasets?keywords=TRMM\_3B42.7&page=1\) \(Huffman et al., 2007\).](https://rda.ucar.edu/datasets/ds728.7/dataaccess/)

## 529 Acknowledgments

530 A.C.N. acknowledges support from Cooperative Institute for Modeling the Earth  
 531 System, AOS, Princeton University, and Geophysical Fluid Dynamics Laboratory (GFDL),  
 532 NOAA. The initial version of the manuscript greatly benefited from discussions and in-  
 533 puts from Dr. Leo Donner and Dr. Bor-Ting Jong. We thank Dr. Yi-Huang Kuo and  
 534 Dr. Issac Held for discussions, Dr. Ming Zhao, Dr. Wenhao Dong and Dr. Huan Gao  
 535 for helping to set up the initial model runs. This work was done by A.C.N. under Award  
 536 NA18OAR4320123 from the National Oceanic and Atmospheric Administration, U.S.  
 537 Department of Commerce. The statements, findings, conclusions, and recommendations  
 538 are those of the author(s) and do not necessarily reflect the views of the National Oceanic  
 539 and Atmospheric Administration or the U.S. Department of Commerce.